



'Quarks' and 'leptons' in three dimensional patterns



Alan C. Newell

Department of Mathematics, University of Arizona, AZ 85721, United States

ARTICLE INFO

Article history:

Available online 30 January 2014

ABSTRACT

The following questions are addressed: How did the symmetries which lead to fractional invariants arise? Can one start with systems with much simpler symmetries, say space translation and rotation, and, by stressing such systems, give rise via phase transitions to objects with natural fractional invariants? Such systems are manifold in nature. They are called pattern forming systems. One has to go no further than one's own fingertips to see examples of two dimensional cross sections of the objects which are the centerpieces of this paper.

© 2014 Elsevier Masson SAS. All rights reserved.

1. Introduction

One of the outstanding successes of modern science has been The Standard Model (TSM) which, among particle physicists, has achieved the status of Abrahamic deities [1]. All beginning letters are capitalized, even in mid sentence. It has provided a theoretical framework for combining three of the four fundamental forces, the electromagnetic, weak and strong, into a unified theory and has laid the groundwork for describing interactions between all subatomic particles, bosons and fermions. The simplest boson is the photon. One of the more complex is the Higgs which is purported to give particles their mass. Recent announcements from CERN indicate that manifestations of the Higgs have been observed. There are twelve elementary fermions, six quarks and six leptons. Among the latter group, the electron is the most familiar example. Combinations of quarks give rise to protons and neutrons. Quarks, whose experimental confirmation in the early 1970s informed the choice of symmetries, namely $U(1)$, $SU(2)$, and $SU(3)$, embedded in TSM, are characterized by their spin (integer multiples of $\frac{1}{2}$) and charge (integer multiples of $\frac{1}{3}$) invariants. Leptons, which also have half integer spins, have unit charges. The Standard Model is also seen as a basis of building more sophisticated models, such as those with super symmetries, which seek to address and explain the presence of the mysterious elements of dark matter and energy.

In this paper, I address a different question. How did the symmetries which lead to fractional invariants arise in the first place? Can one start with systems with much simpler symmetries, say space translation and rotation, and, by stressing such systems, give rise via phase transitions to objects with natural fractional

invariants? While I have no illusions that the story I shall tell will have much impact on particle physics, it is nevertheless interesting that such systems are manifold in nature. They are called pattern forming systems. Indeed, one has to go no further than one's own fingertips to see examples of two dimensional cross sections of the objects which are the centerpieces of this lecture. In the context of epidermal ridge patterns, they are called triradii and loops. More generally, they are recognized in the literature [2] as the canonical point defects of two dimensional patterns, concave and convex disclinations. They are seen widely in many contexts, Rayleigh–Benard convection at high Prandtl numbers [3], ferrofluids [4] and in liquid crystals [5]. Their three dimensional extensions are twisted string-like line defects whose cross sections are concave and convex disclinations. These objects are the main focus of this lecture. They are not simply expressed as algebraic entities, gauge group representations as is the case with the particles in TSM, but as real geometrical objects which can be imagined visually. Indeed, after a lecture I gave in Goettingen about these ideas last year, I learned of a wonderful experiment which has just been reported in a recent issue of *Science* [6] (see also [7]) in which the authors demonstrate the knotting of topological defect lines in chiral nematic liquid crystal colloids which clearly have fractional invariants. The objects we study are also first cousins of the three dimensional spiral or scroll waves observed in excitable chemical media [8] although the latter have integer rather than fractional invariants connected with their well defined circulations $\int_C \vec{k} \cdot d\vec{x}$ of their vector order parameters \vec{k} . Such vortices are also seen in solutions of the three dimensional complex Ginzburg–Landau equation in which context their dynamics have been extensively studied by Aranson, Bishop and Kramer [9,10]. To my knowledge, the only other example of fractionally charged quasiparticles is in the fractional quantum Hall effect [11,12].

E-mail addresses: anewell@math.arizona.edu, royr@email.arizona.edu.

2. Description of patterns far from onset

We focus on externally stressed pattern forming systems which have stripes as their preferred planform and which have no soft or zero (Goldstone or “mean drift”) modes. We will show, first in two dimensions, how concave (V) and convex (X) disclinations spontaneously arise as instabilities and how they are solutions of the field equation which describes the macroscopic behavior of the striped pattern. Their three-dimensional extensions, which we call V and X strings, are constructed by adding loop backbones to these structures in exactly the same manner that the twisted vortices are constructed in excitable media. We begin the story using a toy model for pattern forming systems, the Swift–Hohenberg (SH) equation [13] for the real field $w(\vec{x}, t)$,

$$\frac{\partial w}{\partial t} + (\nabla^2 + 1)^2 w - R w + w^3 = 0. \quad (2.1)$$

We start by summarizing briefly the Cross–Newell (CN) phase diffusion equation [14–16] which captures the slow and macroscopic dynamics of patterns far from onset. The SH equation mimics qualitatively the patterns seen, for example, in Rayleigh–Benard convection at high Prandtl numbers in a horizontal layer of fluid heated from below. In (2.1), R is analogous to the difference between the Rayleigh number R_a and the onset value $(R_a)_c$ at which value the spatially uniform conduction state becomes unstable to striped convective patterns (rolls) which break the translational symmetry of the original system. R_a is a nondimensional measure of the temperature difference across the layer. We can think of the field $w(\vec{x}, t)$ in (2.1) as being the temperature or vertical velocity field at the middle of the layer. Roll solutions, the stable planform for $R > 0$, can be easily calculated as a 2π periodic Fourier cosine series

$$w(\vec{x}, t) = F(\theta; A_n(k, R), k, R) = \sum_{n=1}^{\infty} A_n(k, R) \cos n\theta, \quad (2.2)$$

where F is 2π periodic in θ , the phase $\theta(\vec{x}, t) = \vec{k} \cdot \vec{x} + \theta_0$ and $k = |\vec{k}| = 1$ is the preferred wavenumber (the “one” with the Laplacian in (2.1)). The preferred wavelength is 2π . The direction of \vec{k} is the direction normal to the roll axes. Because it does not matter whether we label the neighboring constant phase contours corresponding to field maxima (minima) as $0, 2\pi, 4\pi$ or $0, -2\pi, -4\pi$, the field must be even in θ . This fact also leads to some crucial topological features of pattern defects. The amplitudes $A_n(k, R)$ are slaved to the wavenumber k by algebraic relations.

Although (2.1) is a purely gradient system, we expect similar behaviors as we describe here to occur in Hamiltonian systems with wave-like patterns induced by adding external forcing through gradient like non conservative terms. But that is for a later study.

Why do natural patterns have defects and why does one need to introduce the notion of phase variation and diffusion? The key realization is that whereas the pattern planform (rolls) and pattern wavelength (2π) are chosen for energetic reasons, the rotational symmetry leaves open the choice of the roll direction \vec{k} . Indeed, in large boxes, (the inverse aspect ratio ε of the system is defined to be the ratio of the wavelength to some macroscopic length such as box size or interdefect distance) where $0 < \varepsilon \ll 1$, local biases due to boundary conditions or variations in the bulk will determine the local orientations of the roll patches. These patches spread and, in two dimensions, they meet, merge and meld along line and at point defects. The line defects are called phase grain boundaries (PGBs) across which the phase is continuous but its gradient, the local wavevector, changes direction. If the change in direction is too much, we show that a nipple instability occurs and leads to the creation of concave–convex point disclination pairs.

An example of such a natural pattern in a ferrofluid is shown at the top right corner of Fig. 2.1. The other parts of the figure show concave and convex disclinations in convection patterns and on counter propagating light beams. The concave disclination on the lower right corner results from a simulation of the SH equation with carefully chosen boundary conditions. The coarsening of such patterns takes a very long time so for all intents and purposes they are stationary.

To describe such patterns analytically, we have to allow for the local wavevector \vec{k} to change slowly almost everywhere in the bulk and also to allow for more sudden changes (shock like solutions) near point and line defects. The Cross–Newell (CN) theory [2,14,15,17], a derivative of Whitham [18] theory for waves, allows us to do this. We seek solutions $w(\vec{x}, t)$ which are modulations of (2.2),

$$w_0(\vec{x}, t) = F\left(\theta = \frac{\Theta(\vec{X}, T)}{\varepsilon}\right) = \sum_1^{\infty} A_n(k, R) \cos n\theta, \quad (2.3)$$

where $\vec{X} = \varepsilon \vec{x}$, $T = \varepsilon^2 t$, $\vec{k} = \nabla_{\vec{x}} \theta = \nabla_{\vec{X}} \Theta$, and ε , $0 < \varepsilon \ll 1$ is the inverse aspect ratio and the small parameter in far from equilibrium situations. Because $\vec{k}(\vec{X}, T)$ changes, (2.3) is no longer an exact solution of (2.1) and corrections

$$w(\vec{x}, t) = w_0(\vec{x}, t) + \varepsilon w_1(\vec{x}, t) + \dots \quad (2.4)$$

must be sought. Because of translational invariance, both $F(\theta)$ and $F(\theta + \delta\theta)$ are exact solutions of (2.1) to leading order. Therefore $\frac{\partial F}{\partial \theta}$ is a symmetry, meaning that it satisfies (2.1) linearized about $w = w_0$. This means that the equations for the iterates w_1, w_2, \dots , whose right hand sides contain terms involving the variations of $\Theta(\vec{X}, T)$ and $\vec{k}(\vec{X}, T)$ with respect to the slow spatial variable and time, must satisfy certain solvability conditions which express constraints on the manner in which the order parameter $\vec{k} = \nabla \Theta$ of the macroscopic system can vary. These solvability conditions can be written as two asymptotic expansions. The first is the amplitude component which, at leading order, gives a system of nonlinear algebraic equations for $A_n(k, R)$ in terms of $A_1(k, R)$ and an algebraic equation for $A_1(k, R)$ in terms of k and R (roughly $(R - (k^2 - 1)^2)A_1 - \frac{3}{4}A_1^3 = 0$). Its corrections at $\varepsilon^2, \varepsilon^4$ involve time and space partial derivatives of A_1 and \vec{k} . They are only important when A_1 is small, that is, near onset when R is small. Near $R = 0$, they combine with the solvability conditions arising at odd powers of ε , the CN phase diffusion equation, to give the familiar Ginzburg–Landau type Newell–Whitehead–Segel equation [19,20] for a complex order parameter $A = A_1 \exp i\theta$. Far from onset, however, there is only one order parameter, the phase or phase gradient, and it satisfies

$$\tau(k) \frac{\partial \Theta}{\partial T} + \nabla \cdot \vec{k} B(k) + \varepsilon^2 \eta \nabla^4 \Theta = 0, \quad (2.5)$$

the regularized CN (RCN) equation. In (2.5), $\tau(k)$ is positive and η is calculable. The interesting structure is contained in the function $B(k)$ which, because of rotational invariance, only depends on k . It is defined for $k_L < k < k_R$, where $k_L(R)$ and $k_R(R)$ are the left- and right-hand boundaries of the neutral stability curve for the instability in (2.1) of the ‘conduction’ solution $w = 0$. The graph of $kB(k)$ is cubic in shape, zero at k_L , positive between k_L and k_0 and negative between k_0 and k_R . k_0 is the single internal zero of $kB(k)$ in (k_L, k_R) and here is equal to one, the preferred wavenumber, although more generally it will depend on R . The graph has a maximum at $k = k_{EL}$ and a minimum at k_{ER} , called the Eckhaus stability boundaries. A little analysis shows that the second order quasilinear partial differential expression $\nabla \cdot \vec{k} B$ in $\Theta(\vec{X}, T)$ is elliptic positive in (k_L, k_{EL}) , hyperbolic in (k_{EL}, k_0) , elliptic negative in (k_0, k_{ER}) , a region called the Busse balloon, and again hyperbolic

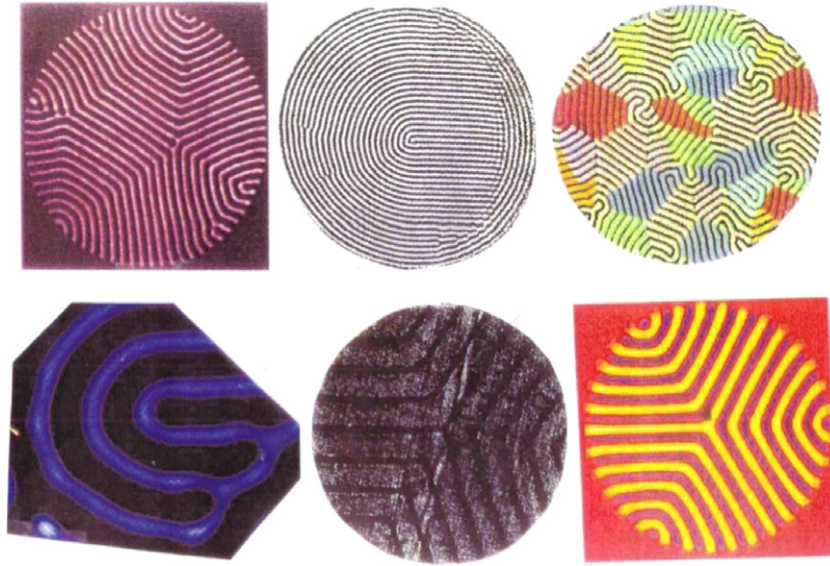


Fig. 2.1. Concave-convex point disclinations in experiments.

in (k_{EL}, k_R) . Since natural patterns have a wavenumber $k = k_0 = 1$ almost everywhere except at line and point defects, at the line and point defects the deviation from 1 is negative (see Fig. 2.1). Therefore if one plots a histogram of wavenumbers in that class of natural patterns for which the SH equation is a useful model, one sees that it has its maximum at a wavenumber slightly below $k = k_0 = 1$. As a consequence, without the correction, Eq. (2.5) is the reverse heat equation along the direction parallel to the local axis of the rolls. Therefore the correction bi-Laplacian is required in the vicinity of those regions where $k < k_0 = 1$ and plays a role entirely analogous to dissipation and diffusion in shock formation situations. It stops the unbounded amplification of small scales and leads to smooth transitions in the wavevector direction along PGBs.

3. Properties of (2.5) in two space dimensions

We now state several properties of Eq. (2.5) in two spatial dimensions. The interested reader can consult the cited Refs. [2,14,15,17,21] for more discussion.

1. It is universal for all pattern forming systems assuming no soft modes, such as the mean drift we would find in moderate to low Prandtl number situations, are present. The graph of $kB(k)$ always has the cubic shape, positive between k_{EL} and k_0 and negative from k_0 to k_{ER} .
2. It inherits the fact that if (2.1) is gradient, then so is (2.5), namely

$$\tau(k) \frac{\partial \Theta}{\partial T} = - \frac{\delta E}{\delta \Theta} \tag{3.1}$$

where

$$E = \int (G^2 + \varepsilon^2 \eta (\nabla^2 \Theta)^2) d\vec{X} \tag{3.2}$$

and

$$G^2 = -2 \int_{k_0=1}^k kB(k)dk.$$

For (2.1),

$$4kB(k) = \frac{d}{dk} \int_0^{2\pi} F^4 d\theta.$$

Indeed $\frac{1}{\varepsilon}E$ is simply the free energy for (2.1) averaged over many wavelengths. One can also derive (3.1) and (3.2) by taking the original free energy for (2.1) and averaging over a pattern period. So E in (3.2) is analogous to Whitham’s averaged Lagrangian in his theory of nonlinear wave modulations. It turns out that even though the Oberbeck–Boussinesq equations for high Prandtl number convection are not exactly gradient, the “averaged” pattern behaves as if they were.

3. Because in many circumstances the wavenumbers k throughout the region are close to the preferred wavenumber, one can often approximate G^2 by $(k^2 - 1)^2$. By rescaling, we can take $\eta = 1$. Then the free energy (2.2) divided by ε is

$$\frac{1}{\varepsilon}E = \int \left(\frac{1}{\varepsilon} (1 - (\nabla \Theta)^2)^2 + \varepsilon (\nabla^2 \Theta)^2 \right) d\vec{X} \tag{3.3}$$

which, after writing $\vec{X} = \varepsilon \vec{x}$, is exactly analogous to the sum of the strain and bending energies for thin elastic sheets with thickness proportional to ε and vertical deformation $\Theta(\vec{X}, T)$ [22].

4. The connection between (3.3) and the family of Ginzburg–Landau minimization problems is given in [17,23]. The challenges in dealing with nonconvex energies and the associated lack of uniqueness are discussed there.
5. We will be searching for minimizers of (3.3) over fields $\Theta(\vec{X}, T)$ and gradients $\nabla \Theta$ which are double valued, namely director fields (vector fields without the arrow!) or vector fields over a double cover of the plane (in two dimensions). The reason for this is the property, mentioned earlier, that we can label neighboring contours of constant phase as either increasing or decreasing by 2π . Mathematically, one can see that given a real field $w(\vec{x}, t) = A \cos \theta$ one can determine θ and $\nabla \theta$ from $w(\vec{x}, t)$ only up to sign. As a consequence, the point defects V , a concave disclination, and X , a convex disclination, shown in Figs. 3.1 and 3.2, have the property that if one follows the “wavevector” on any contour surrounding the point singularity, it twists by $-\pi$ or π . When divided by 2π , these invariant indices are analogous to spins of $\mp \frac{1}{2}$. The minimum energy configuration for a concave disclination will have 120 degree angles between the PGBs.

By contrast, for complex valued fields, such as that occur in systems described by the complex Ginzburg–Landau equation, the phase gradient is determined uniquely by the complex field w and its gradient (e.g. $w = A \exp(i\theta)$). In such



Fig. 3.1. Concave disclination.



Fig. 3.2. Convex disclination.

systems, the defects are loop dislocations and loop vortices with corresponding spins of ∓ 1 corresponding to circulations $\int_C (k \cdot dr)$ of $\mp 2\pi$.

6. The minimization of (3.3) has a wonderful self-dual property. Solutions of the self dual equations

$$\varepsilon \nabla^2 \theta = \pm \sqrt{G^2} \simeq s(1 - (\nabla \theta)^2), \quad s = \pm 1, \quad (3.4)$$

are solutions of the full fourth order Euler–Lagrange equation for (3.2) and (3.3), if the solution (level surface) $\theta(\vec{X}, T)$ has zero Gaussian curvature. The Gaussian curvature for phase grain boundaries is always zero. For disclinations (Figs. 3.1 and 3.2), it resides at the point singularity in each of their centers and is zero elsewhere.

7. The phase grain boundary (PGB) solution: This self-dual property allows us to linearize the Euler–Lagrange equation via the transformation $\theta = \varepsilon s \ln \psi$, $s = \pm 1$ whence (3.4) becomes

$$\varepsilon^2 \nabla^2 \psi - \psi = 0. \quad (3.5)$$

Exact solutions such as $\psi = e^{s\vec{k} \cdot \frac{\vec{x}}{\varepsilon}}$, $|\vec{k}| = 1$, correspond to stripes. A linear combination of exponentials, $\psi = e^{s\vec{k}_+ \cdot \frac{\vec{x}}{\varepsilon}} + e^{s\vec{k}_- \cdot \frac{\vec{x}}{\varepsilon}}$, $|\vec{k}_+| = |\vec{k}_-| = 1$, to a phase grain boundary (PGB) whose direction is $\frac{\vec{k}_+ + \vec{k}_-}{2}$. The phase for the PGB is given by (we write the expression in terms of the original phase θ and space variables $\vec{x}(x, y)$)

$$\theta = \frac{(\vec{k}_+ + \vec{k}_-) \cdot \vec{x}}{2} + s \ln \cosh s \frac{(\vec{k}_+ - \vec{k}_-) \cdot \vec{x}}{2} \quad (3.6)$$

with corresponding wavevector

$$\begin{aligned} \nabla \theta &= (f, g) \\ &= \frac{\vec{k}_+ + \vec{k}_-}{2} + \frac{\vec{k}_+ - \vec{k}_-}{2} \tanh s \frac{(\vec{k}_+ - \vec{k}_-) \cdot \vec{x}}{2}. \end{aligned} \quad (3.7)$$

For $s \frac{\vec{k}_+ - \vec{k}_-}{2} \cdot \vec{x} \geq 0$,

$$\nabla \theta \rightarrow \begin{cases} \vec{k}_+ \\ \vec{k}_- \end{cases} \quad (3.8)$$

The PGB has a boundary layer structure in which the wavevector \vec{k} undergoes a transition from \vec{k}_- to \vec{k}_+ within several wavelengths of the PGB. One can also interpret it as a weak shock

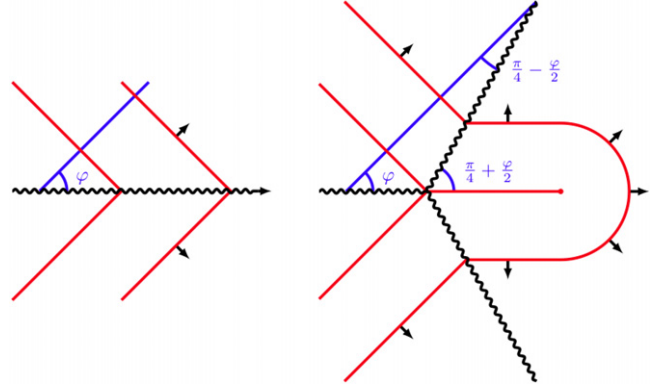


Fig. 3.3. The nipple instability.

solution of the hyperbolic equation $\nabla \cdot \vec{k} B(k) = 0$ which is regularized by the biharmonic term in (2.5) (see [21]). The solutions (3.6) and (3.7) are vector field minimizers of the free energy (3.2). The PGB energy is proportional to $\sin^3 \varphi$ per unit length where $\vec{k}_\pm = (\cos \varphi, \pm \sin \varphi)$. Its energy is also proportional to the mean curvature $\nabla^2 \theta$ of the phase surface integrated over an area containing the PGB.

8. For large enough angles φ , the PGB solution is unstable to a director field perturbation leading to VX pair creation. Why is this? Clearly if $\varphi \rightarrow \frac{\pi}{2}$, the two sets of stripes \vec{k}_+ and \vec{k}_- become parallel to both the PGB (which now becomes a maximum of the real field $w(\vec{x}, t)$) and each other. The fact that they point in different directions does not affect the cost because as we have pointed out, it matters not at all to the real field $w(\vec{x}, t)$ whether the phase contours corresponding to its maxima are labeled $\theta = -2\pi, 0, 2\pi$ or $\theta = 2\pi, 0, 2\pi, \dots$. But according to our formula the cost, proportional to $\sin^3 \varphi$, is maximum at $\varphi = \frac{\pi}{2}$. Therefore one would expect some kind of instability or phase transition to occur when φ reaches a certain value. It does. For large φ , one can significantly lower the energy by making a transition to a director field corresponding to the creation of a VX pair, as shown in Fig. 3.3b. The principal cost in the new configuration arises again from the two PGBs which replace a unit length of the original one. They are longer by a factor of $\frac{1}{\cos(\frac{\pi}{4} + \frac{\varphi}{2})}$ but the angles they make with \vec{k}_+ and \vec{k}_- are $\frac{\pi}{4} - \frac{\varphi}{2}$. Their combined energy is $2 \frac{\sin^3(\frac{\pi}{4} - \frac{\varphi}{2})}{\cos(\frac{\pi}{4} - \frac{\varphi}{2})} = 1 - \sin \varphi$.

This is lower than $\sin^3 \varphi$ when $\varphi \geq 43^\circ$. Therefore, the VX pair configuration is preferred for $\varphi > \varphi_c \simeq 43^\circ$. This instability and VX pair creation marks a distinct departure from the analogy with elastic surfaces. There $\theta = h$, the height of the sheet above a given level, is single valued. Moreover, an elastic surface which is bent along a rooftop requires finite energy. On the other hand, as we have already stressed, a set of parallel rolls at the preferred wavelength requires no energy just because the phase contours are labeled $-4\pi, -2\pi, 0, -2\pi, -4\pi$ rather than $-4\pi, -2\pi, 0, 2\pi, 4\pi$.

9. We emphasize the point: The creation of VX pairs results from a phase transition/instability which occurs when two patches with different orientations (made possible by the rotational symmetry) meet at too sharp an angle. Note that even saddle point singularities, the merging of two concave disclinations, for which the phase grain boundaries are at angles of 45° with respect to the roll wavevectors, are unstable. Far from equilibrium, saddles will disintegrate into two concave disclinations (see Figure 12 in [2]).
10. As R approaches zero, the pattern onset value, at a certain $R_0(\varepsilon)$, which depends on ε , the amplitude becomes an active rather than a passive (slaved) order parameter. It combines

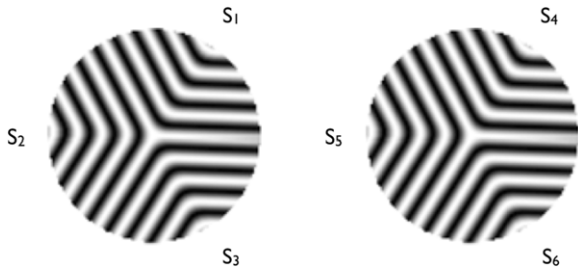


Fig. 3.4. Sectors for a concave disclination.

with the phase to give a complex order parameter and consequently, disclinations, which have double valued \vec{k} values, disappear. The reason is that the complex order parameter $A_1 \exp i\theta$ and its gradient determine $\nabla\theta$ uniquely. Experiments indeed show that they do.

11. Exact multivalued solutions of the stationary hyperbolic equation $\nabla \cdot \vec{k}B(k) = 0$ have been found using a hodograph transformation [2,21]. When regularized using (5), they give the V (concave) and X (convex) disclinations shown in Figs. 3.1 and 3.2. The concave disclinations have three phase grain boundaries and their energy scales with their size L . The convex disclinations require much less energy, proportional in fact to $\ln L$, where L is their size.
12. It is a useful exercise to consider the multivalued solutions of $\nabla \cdot \vec{k}B(k) = 0$ when we set $B(k) = 1$. In this case, the constraint that $k = 1$ almost everywhere is lost but the topological structure of the point defects remains the same. Let $\nabla\theta = \vec{k} = (f, g) = (k \cos \varphi, k \sin \varphi)$ and write $\zeta = \rho e^{i\alpha} = X + iY$ and $\Theta = \text{Im} \frac{2}{3} \zeta^{3/2} = \rho^{3/2} \sin \frac{3\alpha}{2}$. A little analysis shows $f - ig = \rho^{1/2} \exp(i\frac{\alpha}{2}) = ke^{-i\varphi}$. Thus $\varphi = -\frac{\alpha}{2}$. As α travels around the defect at $\zeta = 0$, φ twists by $-\pi$. This is the Laplace concave disclination. The Laplace convex disclination is found by setting $\Theta = \text{Im} 2\zeta^{1/2}$. The Laplace equation disclinations arise in the theory of quadratic differentials.
13. Approximate solution for the concave disclination by six PGBs. For $r = \sqrt{x^2 + y^2} \gg 2\pi$ (the preferred wavelength), the concave disclination can be well represented by six PGBs, three on one plane and three on its cover. Consider Fig. 3.4 which shows two circles split up into six sectors S1–S6, $\frac{2(n-1)\pi}{3} < \alpha < \frac{2n\pi}{3}$, $n = 1, \dots, 6$. Using the formulas given in (11), (12), the corresponding phases wavevectors (written in original coordinates based upon the preferred wavelength scale) are:

$$S1 \quad 0 < \alpha < \frac{2\pi}{3}, \quad \vec{k}_+ = \left(\frac{\sqrt{3}}{2}, \frac{1}{2} \right),$$

$$\vec{k}_- = (0, 1), \quad s = -1$$

$$\theta_1 = \frac{\sqrt{3}}{4}x + \frac{3}{4}y - \ln \left(2 \cosh \left(\frac{1}{4}y - \frac{\sqrt{3}}{4}x \right) \right)$$

$$= \frac{\sqrt{3}}{2}r \cos \left(\alpha - \frac{\pi}{3} \right) - \ln \left(2 \cosh \frac{r}{2} \sin \left(\alpha - \frac{\pi}{3} \right) \right) \quad (3.9)$$

$$(f, g)_1 = \frac{\sqrt{3}}{4} + \frac{\sqrt{3}}{4} \tanh \frac{r}{2} \sin \left(\alpha - \frac{\pi}{3} \right),$$

$$\frac{3}{4} - \frac{1}{4} \tanh \frac{r}{2} \sin \left(\alpha - \frac{\pi}{3} \right)$$

$$\rightarrow \begin{cases} \frac{\sqrt{3}}{2}, \frac{1}{2} & \alpha > \frac{\pi}{3} \\ 0, 1 & \alpha < \frac{\pi}{3} \end{cases} \quad (3.10)$$

$$S2 \quad \frac{2\pi}{3} < \alpha < \frac{4\pi}{3}, \quad \vec{k}_+ = \left(\frac{\sqrt{3}}{2}, -\frac{1}{2} \right),$$

$$\vec{k}_- = \left(\frac{\sqrt{3}}{2}, \frac{1}{2} \right), \quad s = +1.$$

$$\theta_2 = \frac{\sqrt{3}}{2}x + \ln \left(2 \cosh \left(-\frac{1}{2}y \right) \right)$$

$$= -\frac{\sqrt{3}}{2}r \cos(\alpha - \pi) + \ln \left(2 \cosh \frac{r}{2} \sin(\alpha - \pi) \right) \quad (3.11)$$

$$(f, g)_2 = \frac{\sqrt{3}}{2}, \quad \frac{1}{2} \tanh \frac{r}{2} \sin \alpha. \quad (3.12)$$

$$S3 \quad \frac{4\pi}{3} < \alpha < 2\pi, \quad \vec{k}_+ = (0, -1),$$

$$\vec{k}_- = \left(\frac{\sqrt{3}}{2}, -\frac{1}{2} \right), \quad s = -1.$$

$$\theta_3 = \frac{\sqrt{3}}{4}x - \frac{3}{4}y - \ln \left(2 \cosh \left(\frac{\sqrt{3}}{4}x + \frac{1}{4}y \right) \right)$$

$$= \frac{\sqrt{3}}{4}r \cos \left(\alpha - \frac{5\pi}{3} \right)$$

$$- \ln 2 \cosh \frac{r}{2} \sin \left(\alpha - \frac{5\pi}{3} \right) \quad (3.13)$$

$$(f, g)_3 = \frac{\sqrt{3}}{4} - \frac{\sqrt{3}}{4} \tanh \frac{r}{2} \sin \left(\alpha - \frac{5\pi}{3} \right),$$

$$-\frac{3}{4} - \frac{1}{4} \tanh \frac{r}{2} \sin \left(\alpha - \frac{5\pi}{3} \right) \quad (3.14)$$

$$S4 \quad 2\pi < \alpha < \frac{8\pi}{3}, \quad \theta_4 = -\theta_1 (s = +1) \quad (3.15)$$

$$S5 \quad \frac{8\pi}{3} < \alpha < \frac{10\pi}{3}, \quad \theta_5 = -\theta_2 (s = -1) \quad (3.16)$$

$$S6 \quad \frac{10\pi}{3} < \alpha < 4\pi, \quad \theta_6 = -\theta_3 (s = +1). \quad (3.17)$$

14. Approximate solution for a convex disclination. Let $\theta = s \ln \psi$ in (3.1) and obtain (3.5). On the first branch ($s = +1$), the piecewise continuous solution

$$\psi = e^y, x \gg 0, y > 0 \quad \text{or} \quad r > 0, 0 < \alpha < \frac{\pi}{2}$$

$$\psi = I_0(r) \sim \frac{e^r}{\sqrt{r}}, x < 0, r > 0, \frac{\pi}{2} < \alpha < \frac{3\pi}{2}$$

$$\psi = e^{-y}, x \gg 0, -y > 0 \quad \text{or} \quad r > 0, \frac{3\pi}{2} < \alpha < 2\pi \quad (3.18)$$

can be matched in second derivative along $x = 0$ by seeking solutions for $x > 0$ in the form $e^y f(x, y)$ and neglecting the f_{yy} term leading to the heat equation $f_{xx} + 2f_y = 0$ for $f(x, y)$. Solutions can be found which match the expansion of $\frac{e^r}{\sqrt{r}}$ for $|x| \ll y$. The second branch makes the choice $s = -1$.

15. Spin invariant and Gaussian curvature. It is important to note that the expressions given in remarks (13) and (14) are only approximate because the self dual solutions are not exact solutions of the full Euler–Lagrange equation for (3.2). The obstacle is a nonzero Gaussian curvature of the constant phase contour $\theta(x, y) = \text{constant}$. Nevertheless, they contain the correct topologies. Any initial distribution of Gaussian curvature with twist $-\pi$ (in the case of the concave disclination) or $+\pi$ (in the case of the convex disclination) will gather and condense on the singular point at $r = 0$. The twist is defined as

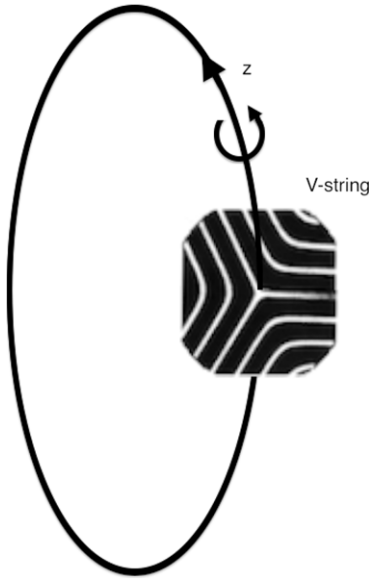


Fig. 4.1. V-string.

the angle by which any straight line with direction $\nabla\theta$ turns on any closed contour surrounding the point singularity at $r = 0$. The twist divided by 2π is called the index. For a concave (convex) disclination the index is $-\frac{1}{2}$ ($+\frac{1}{2}$). The index encodes the area integral of Gaussian curvature of $\theta(x, y) = \text{constant}$. To see this, note that

$$\frac{1}{2\pi} 2 \int_S (\nabla f \times \nabla g) \cdot \hat{n} dS = \frac{1}{2\pi} \int_C (fdg - gdf) \quad (3.19)$$

where \hat{n} is a unit vector to the x, y plane and C is any contour surrounding the origin enclosing the area S . The integrand of the LHS of (3.19) is proportional to the Gaussian curvature of the phase surface $\theta(x, y)$. If we write $f = k \cos \varphi, g = k \sin \varphi$, the RHS is $\frac{1}{2\pi} \int_C k^2 d\varphi$. In the far field, $k \rightarrow 1$. Therefore the RHS is simply $\frac{1}{2\pi} [\varphi]$ where $[\varphi]$ represents the angle through which the direction (f, g) turns as we traverse the contour C . (One can obtain a similar expression for the actual Gaussian curvature but, because $k \rightarrow 1$ in the far field, it is equivalent to (3.19).)

Therefore we see that the spin invariant is related to the condensation of Gaussian curvature at the center of the point defect. We will find in the following section that the “charge” invariant is related to the condensation of the sectional Gaussian curvature along the loop backbone of the string disclination.

4. V and X string defects in three and higher dimensions

Nothing in the theory outlined in Section 3 precludes \vec{k} from being a director field in three or more dimensions. Indeed, one can construct [24] three dimensional point defect analogues of concave disclinations with a tetrahedral skeleton replacing the two dimensional triangular one. Here, however, we focus on a different set of objects we call loop disclinations by attaching backbones to the two dimensional cross sections seen in Figs. 3.1 and 3.2 and asking that the real $w(\vec{x}, t)$ field be periodic in the backbone direction.

Whereas in two dimensions the hodograph transformation linearized the unregularized form of (2.5), $\nabla \cdot \vec{k}B(k) = 0$, in three dimensions we no longer have that simplification. What we do have, however, are:

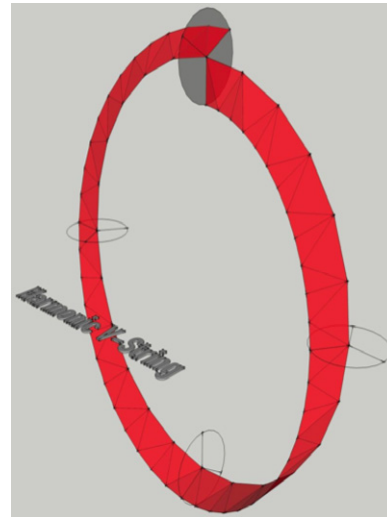


Fig. 4.2. V-string loop.

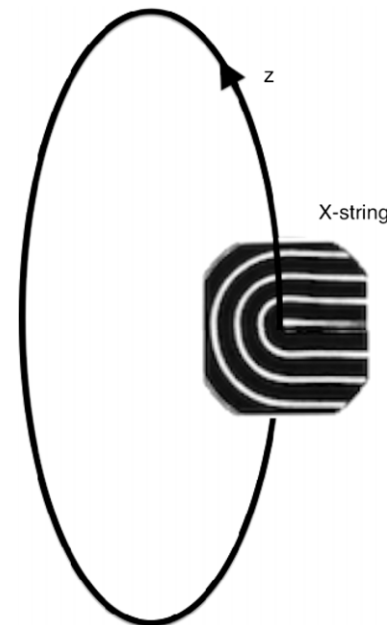


Fig. 4.3. X-string.

- (i) The three dimensional analogues of the harmonic functions $\Theta = \text{Im} \frac{2}{3} \zeta^{\frac{3}{2}}$ and $\Theta = \text{Im} 2\zeta^{\frac{1}{2}}$, $\zeta = X + iY$ obtained by solving Laplace's equation on $S^{(1)} \times R^{(2)}$. These solutions will capture the topology of the defects but not the constraint which chooses the length of the director field to be unity almost everywhere.
- (ii) Approximate solutions to the full RCN equation (2.5)

$$\nabla \cdot \vec{k}B(k) + \eta \nabla^4 \theta = 0 \quad (4.1)$$

obtained by piecing together solutions of the self dual equation

$$\nabla^2 \theta = s(1 - (\nabla \theta)^2), \quad s = \pm 1. \quad (4.2)$$

To obtain (4.2) from (4.1), we approximate $B(k)$ by its Taylor series about $k^2 = 1$ and rescale the spatial variables so as to remove the factor $-\eta/k(\frac{dB}{dk^2})$ estimated at $k^2 = 1$. The self dual solutions are only approximate (they at best provide upper bounds to the associated free energy) because, in addition to the approximation for $B(k)$, they only capture the solution far from the line singularity on the backbone at $r = 0$ on which

nonzero Gaussian curvature is condensed. Nevertheless, they are good in the far field and do possess the correct topologies.

Before we give the results of these calculations, we point out that the main ideas of the two invariants can be seen from a geometrical viewpoint. For the V string, the object of interest is a loop with a concave disclination cross-section which is twisted about the backbone so as to match the $w(\vec{x}, t)$ field at the two ends $z = 0$ and $z = l$ which are identified. This can be done in essentially two ways. We can ask either that the phase field is periodic, i.e. $\theta(x, y, z = 0) = \theta(x, y, z = l)$ or antiperiodic, i.e. $\theta(x, y, z = 0) = -\theta(x, y, z = l)$. To achieve the former we must match sectors S_1 and S_3 , as shown in Fig. 3.4, which will require a twist of the direction $f, g, h = \nabla\theta$ along a suitable contour joining $r = r_0, \alpha = 0, z = 0$ to $r = r_0, \alpha = \frac{4\pi}{3}, z = l$ of $\frac{2}{3} \cdot 2\pi$. To achieve the latter, we simply match sectors of S_1 and S_2 which will require an angular twist of $\frac{1}{3} \cdot 2\pi$. Each of their negatives is also possible by twisting in the clockwise direction. The spin invariant is obtained by examining the twist of the direction $\nabla\theta$ around any cross-section. For the X-string, the field $w(\vec{x}, t)$ can only be made periodic in the backbone direction by twisting the backbone by an integer multiple of 2π . The spin index again is $\frac{1}{2}$. Each invariant is associated with the twist of the director field around the two independent directions on the torus and the line integrals can be related to the area integrals of the two independent and nontrivial sectional Gaussian surface curvatures of the three dimensional surface $\theta(x, y, z)$.

For the V-string, or pattern quarks, the Laplacian approximation can be written as

$$\theta = \frac{2}{3}Kr^{\frac{3}{2}} \sin\left(\frac{3\alpha}{2} - \frac{n\pi z}{l}\right) \tag{4.3}$$

where n is integer and we have approximated $I_{3/2}(r)$ by its small argument limit. Therefore we work in the radial domain $2\pi(=\lambda) \ll r \ll l$.

$$f - ig = Kr^{1/2} \exp i\left(\frac{\alpha}{2} - \frac{n\pi z}{l} - \frac{\pi}{2}\right) \tag{4.4}$$

$$h = -\frac{2\pi n}{3l}Kr^{3/2} \cos\left(\frac{3\alpha}{2} - \frac{n\pi z}{l}\right). \tag{4.5}$$

We note that, for $\frac{r}{l}$ small, $|h| \ll |f|, |g|$. Therefore the twist of the direction (f, g, h) can be calculated from the change in φ where $f - ig = \sqrt{f^2 + g^2} \exp(-i\varphi)$, $\sqrt{f^2 + g^2} = Kr^{1/2}$, and

$$\varphi = -\frac{\alpha}{2} + \frac{n\pi z}{l} + \frac{\pi}{2}. \tag{4.6}$$

Along the contour $z = \text{constant}$, $0 \leq \alpha \leq 2\pi$, the twist or change in φ is $-\pi$. Along the contour $\alpha = \alpha_0 + \frac{2\pi}{3}t, z = \frac{1}{n}t, r = r_0(\alpha_0), 0 \leq t \leq n$ on which θ and h are constants, the change of $\varphi, \frac{1}{2\pi}[\varphi]$ is

$$\frac{1}{2\pi}[\varphi] = \frac{1}{3}n. \tag{4.7}$$

For θ periodic over $0 \leq z \leq l, n$ is even and its smallest value is $n = 2$. We call this the pattern up quark. For θ antiperiodic, we choose $n = 1$. We call this the pattern down quark. The corresponding index is $\frac{1}{3}$.

For X-strings, or pattern leptons, the Laplace solution is $\theta = 2Kr^{1/2} \sin(\frac{\alpha}{2} - \frac{n\pi z}{l})$ for which $f - ig = \sqrt{f^2 + g^2} \exp(-i\varphi) = Kr^{1/2} \exp i(-\frac{\alpha}{2} - \frac{n\pi z}{l} - \frac{\pi}{2}), h = -\frac{2nK\pi r^{3/2}}{l} \cos(\frac{\alpha}{2} - \frac{n\pi z}{l})$. The twist angle is

$$\varphi = \frac{\alpha}{2} + \frac{n\pi z}{l} + \frac{\pi}{2}. \tag{4.8}$$

Around the two circuits $r = r_0, z = \text{constant}, 0 \leq \alpha \leq 2\pi$ and $r = r_0, z = \frac{1}{n}t, \alpha = \alpha_0 - 2\pi t, 0 \leq t \leq n$ the respective twists are π and $-2\pi n$. The choice of antiperiodic θ leads to indices ∓ 1 . We note that the choice θ periodic leads to indices ∓ 2 .

For the V-string, or pattern quarks, the self dual approximation in Sections 1–3 gives

$$S1 \quad \theta_1(r, \alpha, z; n) = \frac{\sqrt{3}}{2}r \cos\left(\alpha - \frac{2n\pi}{3} \frac{z}{l} - \frac{\pi}{3}\right) - \ln\left(2 \cosh \frac{r}{2} \sin\left(\alpha - \frac{2n\pi}{3} \frac{z}{l} - \frac{\pi}{3}\right)\right) \tag{4.9}$$

$$S2 \quad \theta_2(r, \alpha, z; n) = -\frac{\sqrt{3}}{2}r \cos\left(\alpha - \frac{2n\pi z}{3l} - \pi\right) + \ln\left(2 \cosh \frac{r}{2} \sin\left(\alpha - \frac{2n\pi z}{3l} - \pi\right)\right) \tag{4.10}$$

$$S3 \quad \theta_3(r, \alpha, z; n) = \frac{\sqrt{3}}{2}r \cos\left(\alpha - \frac{2n\pi z}{3l} - \frac{5\pi}{3}\right) - \ln\left(2 \cosh \frac{r}{2} \sin\left(\alpha - \frac{2n\pi z}{3l} - \frac{5\pi}{3}\right)\right). \tag{4.11}$$

The sectors are rotated versions of those shown in Fig. 3.4 and are defined by $\frac{2(n-1)\pi}{3} < \alpha - \frac{2n\pi}{3} \frac{z}{l} < \frac{2n\pi}{3}, n = 1-6$. The solutions are approximate, valid for $2\pi \ll r \ll l$. The phase functions $\theta_4, \theta_5, \theta_6$ in sectors 4, 5, 6 are the negatives of those in S1, S2, S3. The z dependence of the arguments are chosen so that, under the twist associated with integer n , the points α_0 on $z = 0$ rotate to $\alpha_0 + \frac{2n\pi}{3}$ on $z = l$. We note that

$$\theta_1(r, \alpha, z = l; n = 2) = \theta_3(r, \alpha, z = 0; n = 2) \tag{4.12}$$

and

$$\theta_1(r, \alpha, z = l; n = 1) = -\theta_2(r, \alpha, z = 0; n = 1). \tag{4.13}$$

In the first case, we match sectors 1 and 3. The twist along the helical contour joining $(r_0, 0, 0)$ to $(r_0, \frac{4\pi}{3}, l)$ is $\frac{4\pi}{3}$. In the second case, the twist is $\frac{2\pi}{3}$. Again the twist along a contour at constant z is $-\pi$.

A similar three dimensional analogue to the two dimensional solutions discussed in remark (15) of Section 5 gives twists for the X-string of π and $-2\pi n$.

There is a connection of the “charge” invariants with the Gaussian curvature of the twisting phase surface that has a boundary which consists of C_1 : a helical curve joining $(r = r_0, \alpha = 0, z = 0)$ to $(r = r_0, \alpha = \frac{4\pi}{3}, z = l)$; C_2 : the straight line at $\alpha = \frac{4\pi}{3}$, joining $r = r_0$ to $r = 0$; C_3 : the backbone on which $k \rightarrow 0$ joining $z = l$ to $z = 0$ at $r = 0$; C_4 : The straight line joining $r = 0, \alpha = 0, z = 0$ to $r = r_0, \alpha = 0, z = 0$. The value of $\frac{1}{2\pi} \int_{C_1} k^2 d\varphi$ is $\frac{2}{3}$. Its value on C_2 and C_4 is zero because on these straight lines $[\varphi] = 0$. The value along the backbone is also zero. Thus $\frac{1}{2\pi r_0} \cdot 2 \int (\nabla f \times \nabla g) \cdot \hat{n} dS$ which adds the projections of $(\nabla f \times \nabla g)$ onto $z = 0, r \leq r_0, 0 \leq \alpha \leq \frac{4\pi}{3}$ and onto $\alpha = 0, 0 \leq r \leq r_0, 0 \leq z \leq l$ is $\frac{2}{3}$. One can calculate these integrals for the case where we approximate θ by $\frac{2}{3}r^{\frac{3}{2}} \sin(\frac{3\alpha}{2} - \frac{2\pi z}{l})$. Then $\frac{1}{r}(f_r g_\alpha - f_\alpha g_r) = -\frac{1}{4r}, f_r g_z - f_z g_r = \frac{\pi}{l}$ and $\frac{1}{r}(f_\alpha g_z - f_z g_\alpha) = 0$. The integral $\frac{2}{2\pi r_0} \int_0^{r_0} \int_0^{\frac{4\pi}{3}} \frac{1}{r}(f_r g_\alpha - f_\alpha g_r) r dr d\alpha = -\frac{1}{3}$ whereas $\frac{2}{2\pi r_0} \int_0^{r_0} \int_0^l \frac{\pi}{l} dr dz = 1$. In the harmonic case, one must divide out by the radius r_0 as the wavenumber k^2 does not tend to unify in the far field but to r .

Therefore the two sets of invariants, the “spins” $-\frac{1}{2}$ and $\frac{1}{2}$ and the “charges” $\pm 1, \pm \frac{2}{3}, \pm \frac{1}{3}$ reflect the amounts of sectional Gaussian curvatures which have condensed on the loop backbones.

On the other hand, the energy of the V string is proportional to the mean curvature condensed along the PGBs for the V-string which is proportional to $3 \sin^3 \frac{\pi}{6}$ times multiplied by the product of its cross sectional and backbone lengths L and l . The X-string energy is proportional to $l \ln L$ (see Figs. 4.1–4.3).

5. Open challenges

There are lots of them. Most are of interest in their own right and aim at gaining a better understanding of the defects contained in natural patterns. Others are motivated by the possibility of connections with the origins of subatomic particles.

1. **The embedding of disclinations in physically reasonable far fields.** Even in two dimensions, this is a challenge. Our calculations in Section 5 of the energy of the concave disclination assume that the three phase grain boundaries have infinite extent. So this brings up the question: Are disclinations finite in size with finite energy and, if so, how do the contributions from the phase grain boundaries (discontinuities in the gradient of the phase field) in the case of the concave disclination and of discontinuities in second derivative (curvature) in the case of convex disclinations decay as r , the distance from the core, increases and how do these objects meld in with physically reasonable far fields? Perhaps they do not. Perhaps they are part of a very slowly coarsening process which only ends after many mergings and when the final defect configuration is of the size of the system and constrained from complete elimination only by boundary constraints. These questions become even more difficult when we consider the V and X strings in three dimensions. Can they be embedded in $R^{(3)}$ or do they require the notion of a wrapped up dimension so that the configuration space is not $R^{(3)}$ but $S^1 \times R^{(2)}$ or more simply a torus?

One can try to think of gedanken experiments. In [21], we showed how a striped convective pattern evolves in an elliptical cylinder whose sidewalls are heated. Near the boundary, the convection rolls are parallel to the walls (their wavevector \vec{k} is normal to the wall) and their wavelength is the preferred value, the eikonal construction. But the normals to an elliptical cylinder form caustics emanating from the two foci so that the eikonal solution leads to multivaluedness. A thin film elastic blister would regularize this solution by introducing a wedge-like boundary roof layer between the two foci and allowing the gradient of the height undergo a sharp discontinuity (PGB) there [17]. The angle between the wavevector and the PGB, φ , is zero at both foci and increases towards the center. What we find in a convecting fluid is that, once $\varphi > 43^\circ$, the pattern exercises its option to allow director field perturbations of what was previously a vectorfield. There is a creation of VX pairs, a nipple instability, a prediction supported by both numerical and experimental confirmations, the former using both the Swift–Hohenberg approximations and the full Oberbeck–Boussinesq equations. The final pattern (presumably the energy minimum although, for nonconvex problems, one has no uniqueness result; in some circumstances, one can show by finding almost coincident upper and lower bounds that an observed configuration has an energy which the minimum must have) consists of what appears to be a chain of “dislocations” in which $\nabla\theta \cdot \hat{n}$ and θ are both zero on alternating segments on the chain axis [25]. The number is determined by how strongly elliptical the container is. In an experiment conducted by Ahlers and colleagues, there is only one. It would be interesting to attempt an experiment in an ellipsoidal container, axisymmetric around its long axis, with some pattern producing system, possibly chemical in nature, which can produce three dimensional patterns. One might conjecture that one would obtain a bound

zero charge pair of VX strings because there is no twist along the backbones. It might be also possible to use a toroidal cylinder with elliptical cross section in which one might induce a 2π twist, a hydrogen atom like arrangement.

2. **Interstring forces.** Whereas much is known about the interaction energies and forces between vortices (a back to back superposition of two convex disclinations) and dislocations (two concave, two convex dislocations) in vectorfield pattern forming systems, and, in certain cases, between disclinations in two dimensions, nothing is yet known about the interaction forces between loop disclinations. Some of the difficulty is that we do not have finite energies for individual disclinations. What one would like to be able to calculate is the interaction free energy between two such objects by subtracting the individual free energies from that of the combination and calculating its dependence on the parameters r , an appropriate choice of interdisclination distance, and the spin and charge indices. One would like to see whether, for example, the interactive energy between a single V-string with 2π twist (two up quarks and one down quark) and an X string is inversely proportional to r and the product of the signed charges.
3. **Composites of pattern quarks and leptons.** A related question concerns the composition of pattern quarks and leptons. Presumably one cannot match an individual up or down pattern quark with a pattern lepton because their charges (which are related to their topological structures) do not match. Therefore, one might conjecture that if pattern quarks and leptons can only appear (stably) in pairs then we require quark composites whose indices add to multiples of ± 1 , e.g. two up quarks and a negative down quark (a pattern proton). One could also add a zero charge configuration, e.g., integer multiples of one up and two down quarks (a pattern neutron). Do such composites consist of pattern up and down quarks which share the same loop backbone (and whose topologies are clearly calculated by the addition of indices) or can one have interlinked loops? We should note that their cousins in excitable media, vortices with vectorfield order parameters, tend to appear as single rather than interlinked loops.
4. **More sophisticated models.** Patterns can arise as stationary (exchange of stabilities) or as traveling standing waves (overstability). The latter arise when the unstressed system supports oscillatory or wave motion. For example, the next most simple model of atmospheric motion is the beta plane model which adds the north–south dependence of Coriolis parameter to the geostrophic balance. When stressed with a north–south temperature gradient, the resulting vertical shear of the east–west velocity and associated density, pressure fields can destabilize via what is called the baroclinic instability to a traveling pattern which has the character of Rossby waves, the natural oscillations of the unstressed system. Therefore the recipe for a pattern forming system with waves is a superposition of Hamiltonian and gradient flows. It would be interesting to investigate the nature of defects in a pattern forming system whose Hamiltonian component had Lorenz symmetry added to that of translation and rotation. The system is stressed by the addition of the gradient component.
5. **Giving free rein to the imagination.** Imagine that the soup of all subatomic particles was created in a rapidly expanding universe with only the simplest symmetries and a decreasing temperature acting as stress parameter. As the expanding cloud cools, the uniform state becomes unstable. Patterns are seeded locally with preferred length scales but arbitrary directions. Their merging creates families of elementary defects and their composites whose physical characteristics (mass/energy, charge, spin) are related to the geometry of the phase surfaces from which they are composed. The increasing complexity of

the geometry gives rise to an increasing complexity of the nature of the elementary particles.

In such a scenario, how would the basic scales be chosen and to what realities might they correspond? The preferred scale of the pattern? If waves are involved perhaps a preferred frequency and some relation between pattern amplitude, wavelength and frequency? The length of strings, large compared to the preferred wavelength but very small compared to the diameter of the expanding universe? If no far field constraint exists such as a nontrivial twist index on some boundary, then all twists would be local and the pattern would tend to coarsen with larger and larger interdefect (particle) distances. What would determine the coarsening rate?

But, enough of the speculation. It is time to get down to the hard work of addressing the challenges raised in remarks 1 and 2.

Acknowledgments

This work was supported by the NSF under DMS grant 1308862 and by the Air Force Office of Scientific Research (AFOSR) Multidisciplinary University Research Initiative (MURI) grant FA 9550-10-1-0561. It is dedicated to Enok Palm, a pioneer in the study of patterns arising in geophysical contexts. An earlier version of these ideas was published in [26]. I also want to express my appreciation to all those colleagues (in particular Nick Ercolani, Shankar Venkataramani, Yves Pomeau, Volodja Zakharov and Thierry Passot) who were willing to listen to whacky ideas with tolerance and a healthy mixture of encouragement and hard nosed criticism and skepticism.

References

- [1] D.J. Griffiths, *Introduction to Elementary Particles*, second ed., Wiley, New York, 2008.
- [2] T. Passot, A.C. Newell, Towards a universal theory of patterns, *Physica D* 74 (1994) 301–352.
- [3] Eberhard Bodenschatz. Private communication.
- [4] M. Seul, L. Monar, L. O’Gorman, R. Wolf, Morphology and local structure in labyrinthine stripe domain phase, *Science* 254 (1991) 1557–1696.
- [5] L. Kramer, W. Pesch, Convection instabilities in nematic liquid crystals, *Ann. Rev. Fluid Mech.* 27 (1995) 515–541.
- [6] U. Tkalec, M. Ravnik, S. Copar, S. Zumer, I. Musevic, Reconfigurable knots and links in chiral nematic colloids, *Science* 333 (2011) 62.
- [7] S. Copar, S. Zumer, Nematic braids: topological invariants and rewiring of disclinations, *Phys. Rev. Lett.* 106 (2011) 177–801.
- [8] A.M. Pertsov, R.R. Aliev, V.I. Krinsky, Three dimensional twisted vortices in an excitable chemical medium, *Lett. Nat.* 345 (1990) 419.
- [9] I.S. Aranson, A.R. Bishop, Instability and stretching of vortex lines in the three dimensional complex Ginzburg–Landau equation, *Phys. Rev. Lett.* 79 (1997) 4174–4177.
- [10] I.S. Aranson, L. Kramer, The world of the complex Ginzburg–Landau equation, *Rev. Modern Phys.* 74 (2002) 99–143.
- [11] R.B. Laughlin, Anomalous quantum Hall effect: an incompressible quantum fluid with fractionally charged excitations, *Phys. Rev. Lett.* 50 (1983) 1395.
- [12] H.L. Stormer, Nobel lecture: the fractional quantum Hall effect, *Rev. Modern Phys.* 71 (1999) 875.
- [13] M.C. Cross, P.C. Hohenberg, Pattern formation outside of equilibrium, *Rev. Modern Phys.* 65 (3) (1993) 851–1111.
- [14] M.C. Cross, A.C. Newell, Convection patterns in large aspect ratio systems, *Physica D* 10 (1984) 299.
- [15] A.C. Newell, T. Passot, M. Souli, The phase diffusion and mean drift equations for convection at finite Rayleigh numbers in large containers, *J. Fluid Mech.* 220 (1990) 187–252.
- [16] P. Manneville, Y. Pomeau, Stability and fluctuations of a spatially periodic convection flow, *J. Phys. (Paris) Lett.* 40 (1979) 609–612.
- [17] N. Ercolani, R. Indik, A.C. Newell, T. Passot, The geometry of the phase diffusion equation, *J. Nonlinear Sci.* 10 (2000) 223.
- [18] G.B. Whitham, *Linear and Nonlinear Waves*, John Wiley and Sons, New York, 1974.
- [19] A.C. Newell, J.A. Whitehead, Finite bandwidth, finite amplitude convection, *J. Fluid Mech.* 38 (1969) 279–303.
- [20] L.A. Segel, Distant side-walls cause slow amplitude modulation of cellular convection, *J. Fluid Mech.* 38 (1969) 203–224.
- [21] N. Ercolani, R. Indik, A.C. Newell, T. Passot, Global description of patterns far from onset: a case study, *Physica D* 184 (2003) 127–140.
- [22] M. Ortiz, G. Gioia, The morphology and folding patterns of buckling driven thin film blister, *J. Mech. Phys. Solids* 42 (1994) 531–559.
- [23] F. Bethuel, H. Brezis, F. Hélein, *Ginzburg–Landau Vortices*, Birkhäuser, Boston, 1994.
- [24] A.C. Newell, T. Passot, C. Bowman, N.M. Ercolani, R. Indik, Defects are weak and self-dual solutions of the Cross–Newell phase diffusion equation for natural patterns, *Physica D* 97 (1996) 185–205.
- [25] N. Ercolani, S. Venkataramani, A variational theory for point defects in patterns, *J. Nonlinear Sci.* 19 (2009) 267–300.
- [26] A.C. Newell, Pattern quarks and leptons, *Appl. Anal.* 91 (2) (2012) 213–223.